Thermal Analysis of Small Re-entry Probe

Parul Agrawal[1], Dinesh K. Prabhu[2]

ERC Inc., C/O NASA Ames Moffett Field,CA-94035.

and

Y.-K.Chen[3]

NASA Ames Research Center, Moffett Field, CA, USA 94035-0001

The <u>S</u>mall <u>P</u>robe <u>R</u>eentry <u>I</u>nvestigation for <u>TPS</u> <u>E</u>ngineering (SPRITE) concept was developed at NASA Ames Research Center to facilitate arc-jet testing of a fully instrumented prototype probe at flight scale. Besides demonstrating the feasibility of testing a flight-scale model and the capability of an on-board data acquisition system, another objective for this project was to investigate the capability of simulation tools to predict thermal environments of the probe/test article and its interior. This paper focuses on finite-element thermal analyses of the SPRITE probe during the arcjet tests. Several iterations were performed during the early design phase to provide critical design parameters and guidelines for testing. The thermal effects of ablation and pyrolysis were incorporated into the final higher-fidelity modeling approach by coupling the finite-element analyses with a two-dimensional thermal protection materials response code. Model predictions show good agreement with thermocouple data obtained during the arcjet test.

Nomenclature

CFD   =   computational fluid dynamics
CTE   =   coefficient of thermal expansion
DAS   =   earth entry vehicles
DPLR   =   data-parallel line relaxation
FE   =   finite-element
MMEEV =   multi mission earth entry vehicles
PICA   =   phenolic impregnated carbon ablator
SPRITE =   small probe re-entry investigation for TPS engineering
TC   =   thermocouple
TITAN =   two-dimensional implicit thermal response and ablation
TPS   =   thermal protection system

I.   Introduction

RE-ENTRY probes are designed to bring samples from outer space to earth. During the entry, they experience significant aerothermal heating. In order to protect the vehicles, a layer of ablative and/or insulative thermal protection materials is used at the exterior surfaces. The relatively low conductivity of thermal protection materials causes a slow absorption of thermal energy into the interior of these probes. It could take several minutes to hours before the internal substructure and payload of the vehicle start to show a rise in temperature. These probes land in a very remote area and the recovery process could take several hours. Therefore, thermal soak analysis becomes very important to predict the survivability of the payload.

---

[1] Senior Research Scientist, Thermal Protection Materials Branch, MS 234-1, NASA Ames Research Center, Member AIAA.
[2] Senior Research Scientist, Aerothermodynamics Branch, MS 230-3, NASA Ames Research Center, Associate Fellow AIAA.
[3] Aerospace Engineer, Aerothermodynamics Branch, MS 230-2, NASA Ames Research Center, Member AIAA.

Scientists and engineers at NASA are working to create a common design and analysis tool for earth entry vehicles that would provide design parameters, trajectory and aerothermal heating estimates and materials recommendations for any given mission.[1] One of the objectives for this project is to estimate the temperature history and peak temperature for payloads. The present work focuses on the thermal-soak analysis of SPRITE probe that serves as a first validation experiment to develop this capability. SPRITE is a novel concept that was developed at NASA Ames to enable arc-jet testing of full scale flight models.[2] There were three main objectives for the SPRITE project[3]:

1. To demonstrate the feasibility of arc-jet testing flight articles at full scale – a required first step in the 'test what you fly' paradigm;
2. To demonstrate the feasibility of *in situ* measurements of temperature, strain and recession using a data acquisition system mounted inside the test article, i.e., to demonstrate gathering and storage of data acquired by sensors during an arc jet test; and
3. To demonstrate the ability of a combination of simulation tools, primarily DPLR,[4] TITAN,[5] and MSC.Marc,[6] to predict material response and thermal environments in the interior of the test article during arc jet testing.

To achieve the above objectives, two 0.35 meter diameter models were fabricated at NASA Ames Research Center. These models consisted of a PICA forebody, LI-2200 back shell and metallic substructure as shown in Figure 1. Both the models were instrumented with several thermocouples inside the TPS and at the substructure to obtain temperature histories during and after the arc-jet plasma exposure. The data from the thermocouples (TC) were obtained by two methods: 1) using the onboard data acquisition system (DAS), that was also assumed to be the payload and 2) through arc-jet data acquisition system. The onboard data acquisition system was a unique and novel approach that was adopted for this test. Details of the hardware implantation inside the SPRITE probe are provided in Reference 7. The data acquisition system was powered by two Lithium-Iron polymer batteries with an operating temperature limit of 60°C. Therefore, it was critical to design the test parameters and fabricate the model in such a way that the battery would not overheat (and possibly explode). Extensive finite-element (FE) modeling was performed to provide guidelines for the probe design, material selection, and test conditions. The next two sections summarize the development of the finite-element model and results during the pre-test design phase. The later sections describe a higher-fidelity modeling approach to predict the temperature history of the substructure, batteries, and containment box.
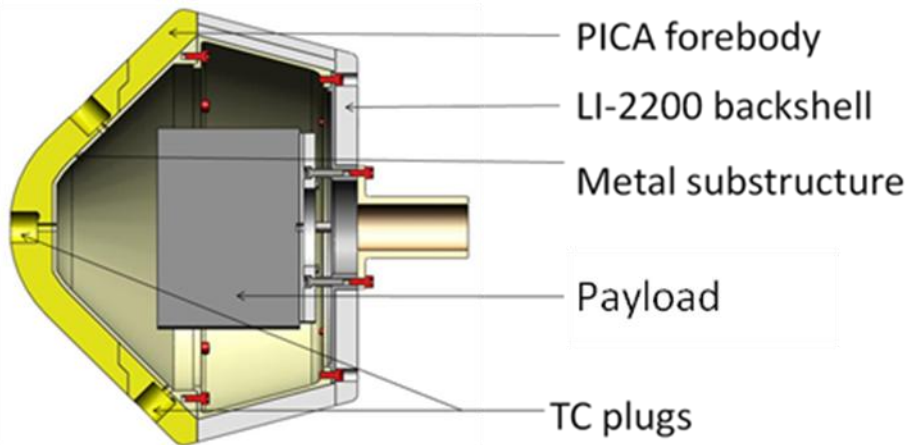

Figure 1: SPRITE model configuration.

II.   Analytical Approach and Model Development

The aeroshell of the SPRITE arc-jet test article was designed to be axi-symmetric. Therefore, for the flow field analysis the body was assumed to be axi-symmetric that generated axi-symmetric heat-flux on the body.   These assumptions led the creation of a 2D axi-symmetric finite-element models to perform thermal analyses. The model dimensions and architecture were based on the actual arc-jet model drawings, shown in Figure 2. All of the thermal analyses for this probe were performed using the MSC.Marc commercial finite-element analysis package.[6]

MSC.Marc supports fully transient, non-linear, thermal finite-element analysis. Non-linear and temperature dependent material properties can be incorporated inside the model. The package allows the application of a wide range of thermal boundary conditions including heat flux and temperatures.

The first set of analyses was performed to help develop the design concepts, material selection and arc-jet exposure time. For these analyses, conduction, external re-radiation and cavity re-radiation were modeled for transport of thermal energy; ablation and pyrolysis were not taken into consideration. This approach provides higher temperature estimates, causing more thermal energy to soak inside the system. The finite-element model used to perform these analyses is shown in Figure 3. The model was meshed with 2D quadratic elements. The heat flux distribution on the outer surface of the forebody and back-shell during the arc-jet exposure was obtained from computational fluid dynamics (CFD). The detailed flow-field analysis of this probe is discussed in Reference 8. The spatially varying heat flux was directly imposed on the finite-element model as a thermal boundary condition. Temperature dependent thermal properties were used for PICA[9] and LI-2200[10]. The 3 mm thick metal substructure was directly bonded to the fore and aft body and full thermal contact between TPS and sub-structure was maintained. For thermal analysis, it was assumed that the very thin adhesive layer between the sub-structure and TPS did not significantly absorb thermal energy and it was not included in the finite-element model. A cylindrical container box, with approximately same dimensions and mass as originally conceived for the DAS container box, was created for the pretest analysis. Inside this container, the DAS board was attached to the box. At the time of pretest analysis, the box design, materials and insulation for the electronics were not finalized so this model was based on early concepts to perform parametric and sensitivity studies and provide guidance for the final design. The heat generated during the battery operation was imposed as a thermal heat flux generation during the entire operation on the DAS board itself. The interior assembly was also modeled as an axi-symmetric body. The container box was insulated from the metallic substructure by means of a Teflon ring as shown in Figure 3. The container box and Teflon ring was attached to the substructure by means of several stainless steel screws. In order to model the thermal pathways in the presence of these screws, an equivalent stainless steel mass was attached from the Teflon plate to the substructure. The internal environment of the probe was assumed to be in vacuum. The primary heat transfer mechanisms were conduction and internal cavity re-radiation.

A higher-fidelity finite-element thermal model was subsequently developed for more accurate predictions of temperature histories on the payload and the probe itself during the cool-down process. In order to account for ablation and pyrolysis during the arc-jet exposure, the temperature distribution predicted by the two-dimensional material response code TITAN[5] was imposed on the finite-element model as initial condition for the cool-down analysis. A built-in user subroutine feature in Marc was used for temperature mapping from TITAN to the finite-element model. To implement accurate temperature maps on the finite-element model, the elements for the aeroshell and substructure were generated using the grid points from TITAN analysis. This approach resulted in a very fine mesh near the surface to account for a very steep temperature gradient during and immediately after the exposure. The temperature variation in the in-plane direction was not as large compared to through-the-thickness, therefore elements with large aspect ratios still led to good convergence of the solution. Based on the density distribution from the TITAN analysis, the elements on the forebody were designated as charred or virgin PICA. The temperature dependent thermal properties for virgin and charred PICA, LI-2200, Al-6061 were used as material inputs for accurate analysis.[9,10] The finite-element model with all the components is shown in Figure 4. The internal components of the probe were created based on the drawings of the electronic container box design, batteries, delrin shelves and DAS board. Even though the container in the 2D axi-symmetric model had the shape of a cylinder rather than a prism, the mass, height and thickness were matched to the real dimensions in order to have the same thermal mass. The energy dissipated by the battery during the operation was also modeled as heat generation during the exposure and entire cool-down period.

The results from the simulations for above mentioned models and comparison with the experimental thermocouple data are discussed next.
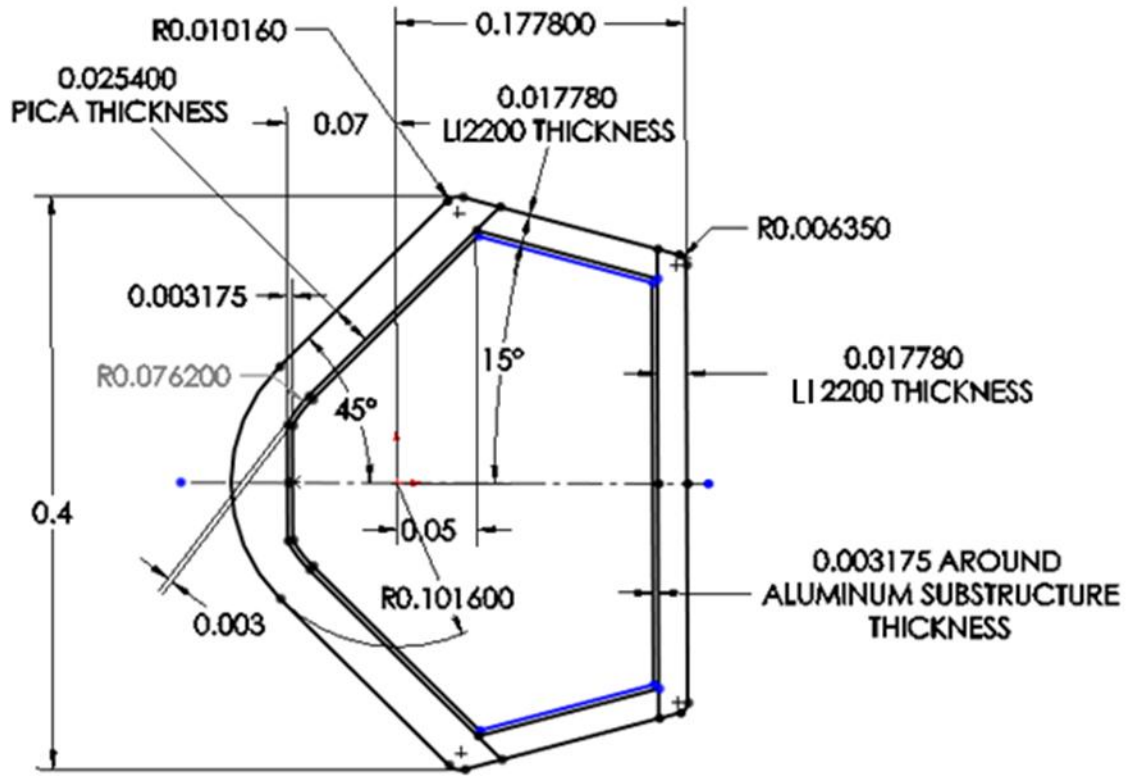
Figure 2: Drawing of the SPRITE probe with dimensions represented in meters.
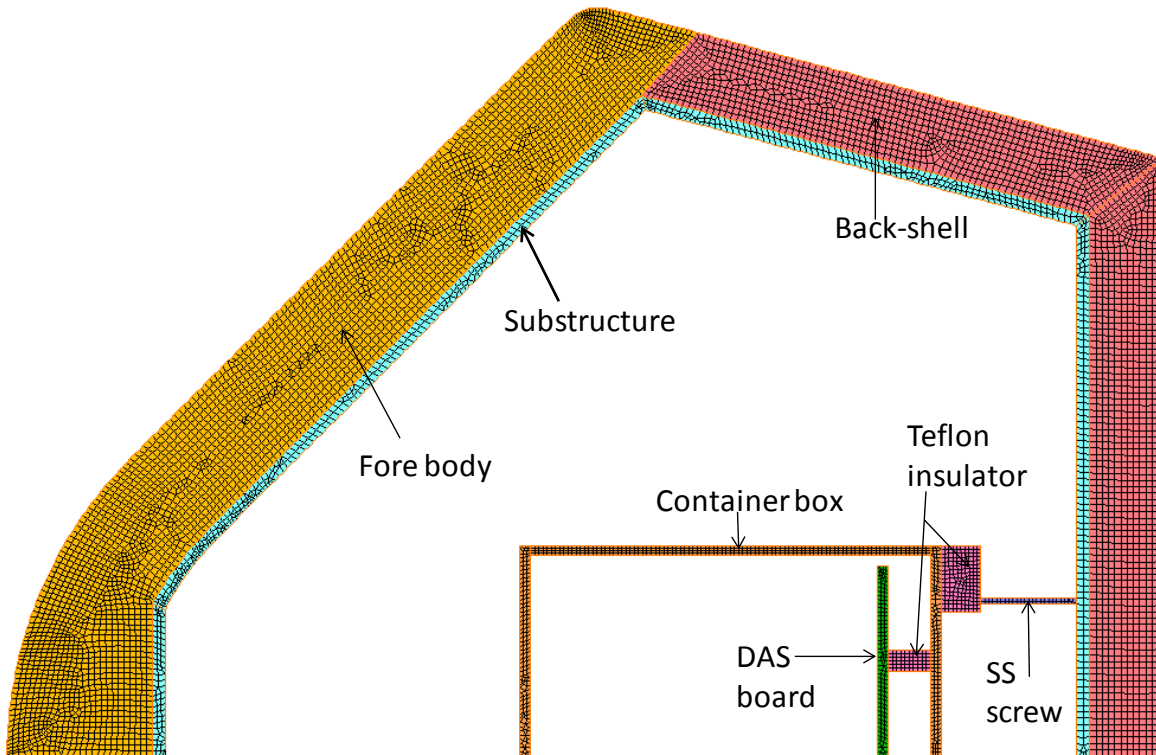

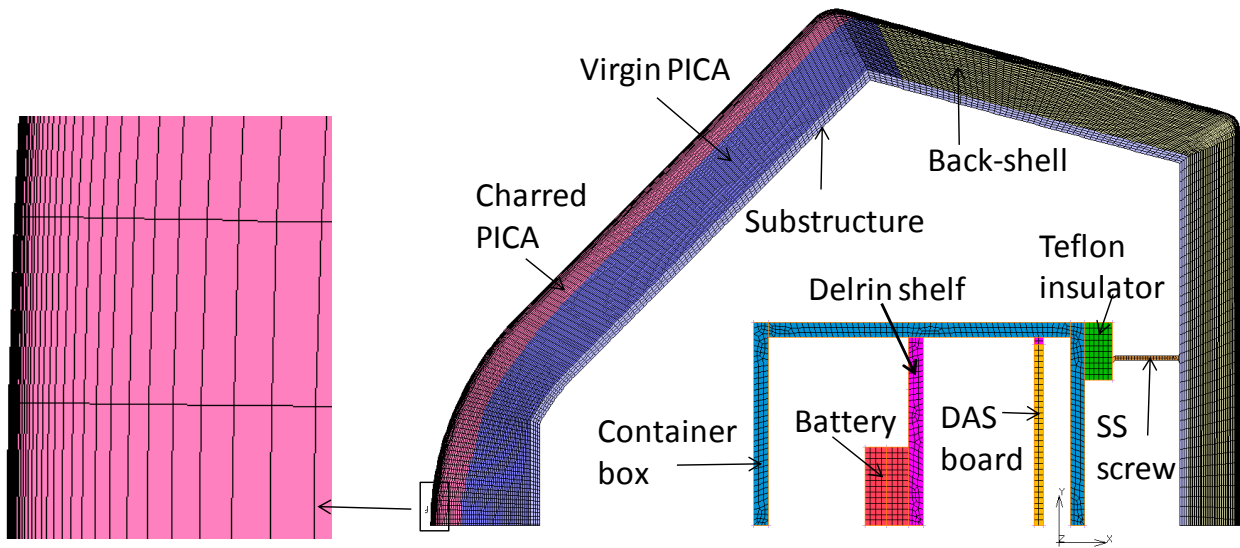**Figure 3: conduction based model for parametric studies.**

Figure 4: High fidelity thermal soak model

III.   Pre-test Analysis

This section summarizes results of simulations performed during the early design phase for the SPRITE project. These simulations provided the first insight into temperatures inside the probe and were performed to help guide the test and design teams in: 1) selecting the material for the substructure and container box for the data acquisition system, 2) determining the exposure time for arc-jet test article, and 3) determining thermal pathways for suitably placing thermocouples in the test article. As mentioned earlier, for the parametric studies the simulations were performed based on heat transfer due to conduction, external re-radiation and internal cavity re-radiation. The heat flux distribution on the surface of the probe during the arc-jet exposure was obtained by DPLR CFD analysis. The heat-flux distribution along the radial coordinates, with both cold wall (cw) and hot wall (hw) assumptions is shown in Figure 5. In the cold wall assumption the wall temperature stays constant at 127°C. In contrast the hot wall assumption takes into account the instantaneous wall temperature during the analysis. For parametric analyses the hot wall heat flux values were imposed as a surface boundary condition to the finite-element model.

At this stage the ablation and pyrolysis of PICA was not accounted, which made the temperature estimates higher than experimentally obtained data. In order to select a suitable material for the substructure, the simulations were performed for both aluminum and titanium (Ti) alloys. The comparison of peak temperatures for 100 seconds of arc-jet exposure for both substructures is shown in Figure 6. The peak temperatures are significantly higher for titanium based substructure than for aluminum that has higher thermal conductivity. The thermal conductivity of Ti alloy is in the range of 7.0 W/mK compared to 160 W/mK for aluminum alloy, whereas; the difference in specific heat capacity for both the alloys is not as large. Therefore, the Ti alloy based substructure stores more thermal energy over time and shows higher temperatures. The aluminum carrier structure dissipates the thermal energy faster and was recommended for the probe, taking higher thermal efficiency and reduced material cost into consideration.

To optimize the design of the DAS container box and insulation, parametric studies were conducted on different materials for the box and insulation around the DAS board. Figure 7 compares the peak temperatures for aluminum and ultem container boxes. As in the case of the substructure, it was found that insulative materials, like ultem, tend to store thermal energy over time and show higher peak temperature. Aluminum was found to be a better material option for the container. It was also found that the best way to dissipate stored energy from the board and battery was not to cover it with insulative blanket and instead to let the energy dissipate via radiation. A comparison of the temperature rise in the DAS board when wrapped with felt insulation versus a more open Teflon support is shown in Figure 8. The peak temperature in the presence of insulation felt blanket was 50°C higher compared to a more open Teflon base.

Arc-jet exposure time was another crucial parameter that was determined by thermal finite-element analyses. The main constraints on the system that drove exposure time estimation were temperature limits for the battery and the substructure. The battery temperature limit was 60^{0}C. The substructure temperature limit was 200^{0}C to avoid excessive thermal stresses due to the coefficient of thermal expansion (CTE) mismatch between the TPS material and substructure. Simulations were performed for arcjet exposure times of 50, 75, and 100 seconds. Figures 9 and 10

American Institute of Aeronautics and Astronautics

show the comparison of temperature histories in substructure and payload respectively, for 50 and 100 seconds exposures. For the 50 second exposure, both the carrier structure and the battery remained below their temperature limits. Based on the temperature histories of the substructure and the DAS board, 50 seconds of exposure time was selected for the arc-jet experiments. The next few sections describe the arc-jet test and temperature histories at different locations of the probe.
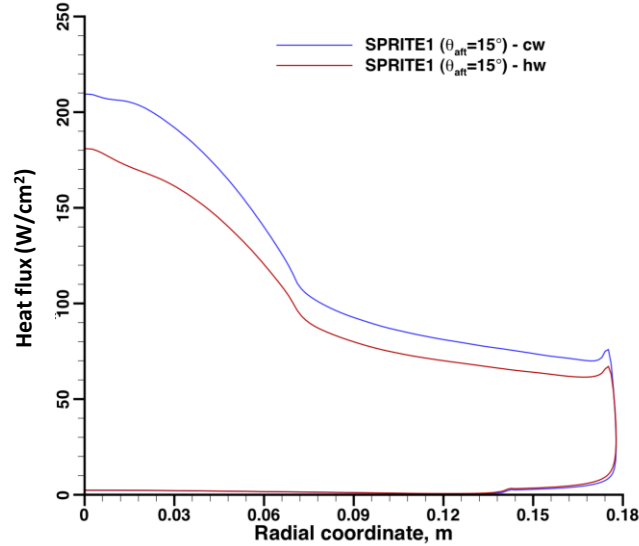

Figure 5: Radial Heat flux distribution from DPLR CFD calculations.
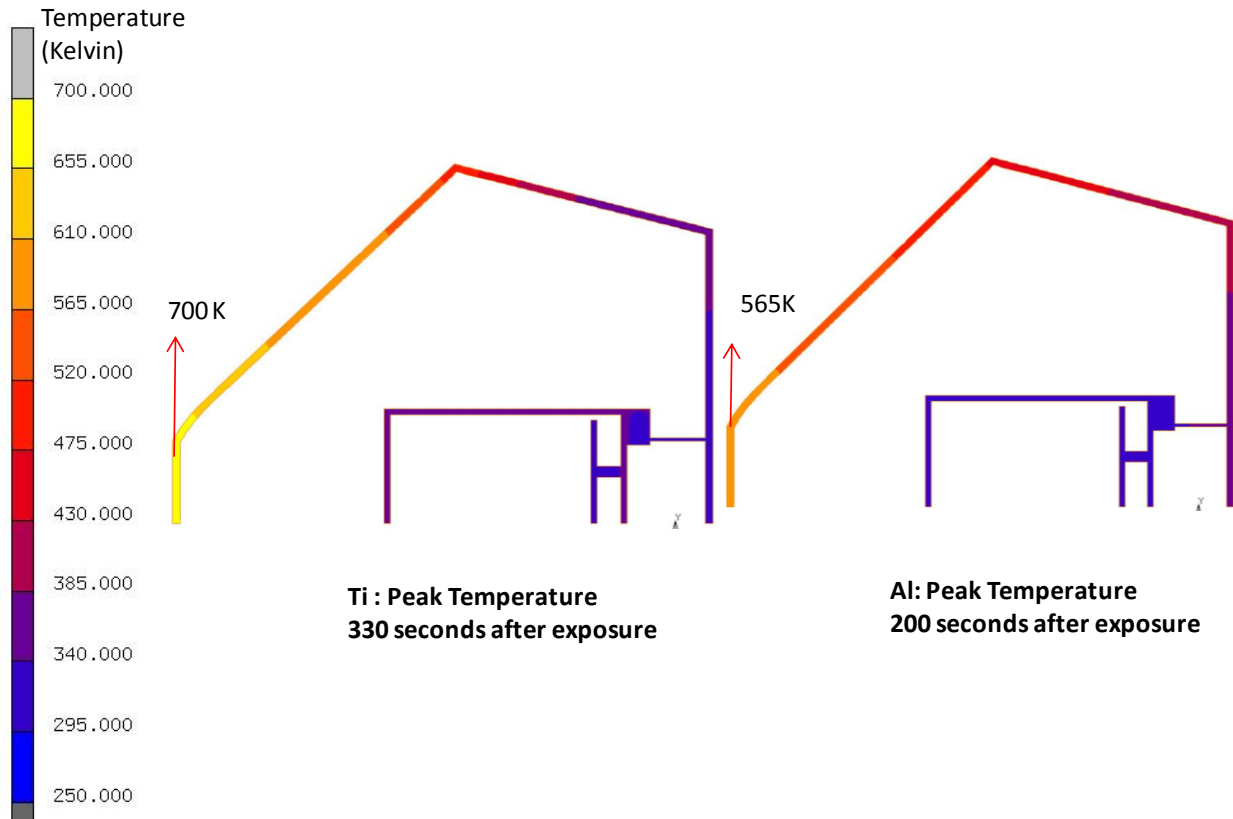
Figure 6: Peak temperature comparison in Ti and Al substructure for 100s of arc-jet exposure.
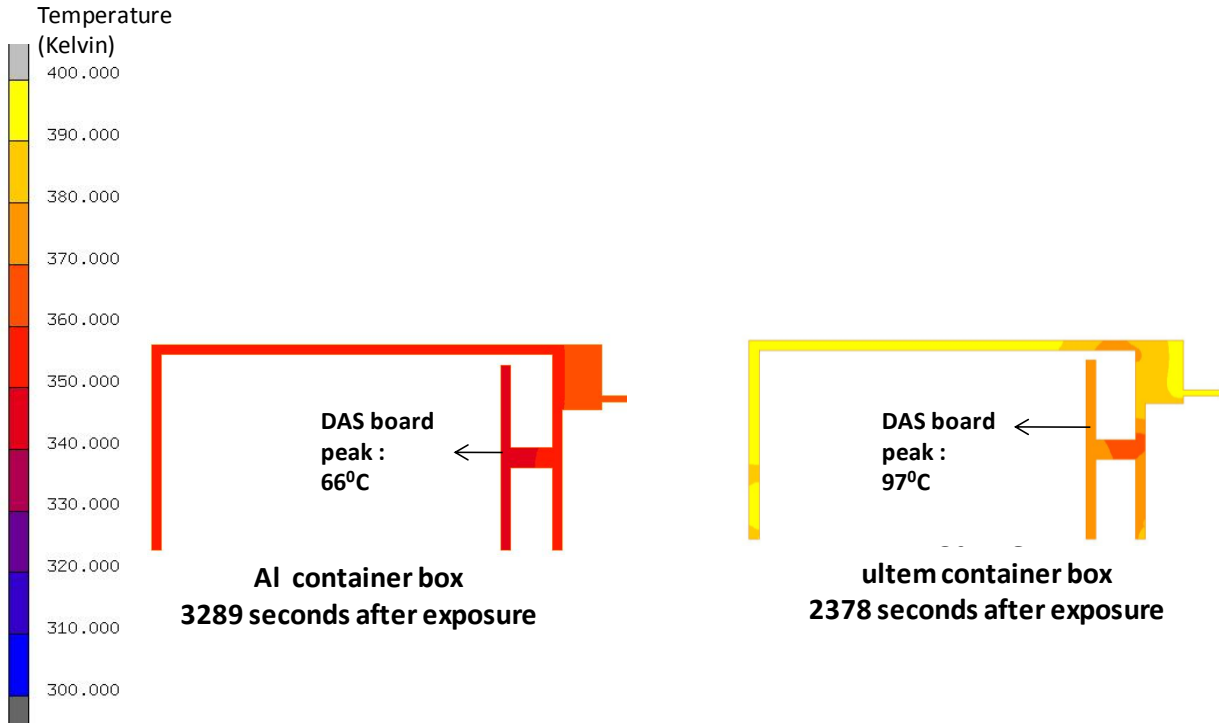
Figure 7: Peak temperature comparison in Al and ultem container box for 100s of arc-jet exposure.
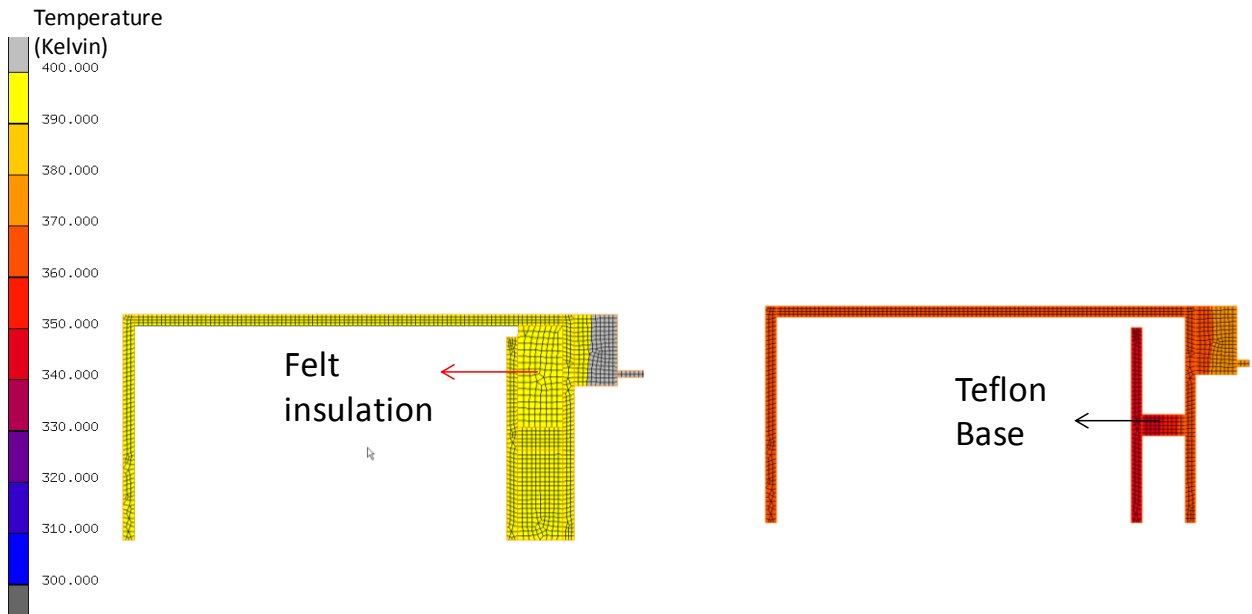

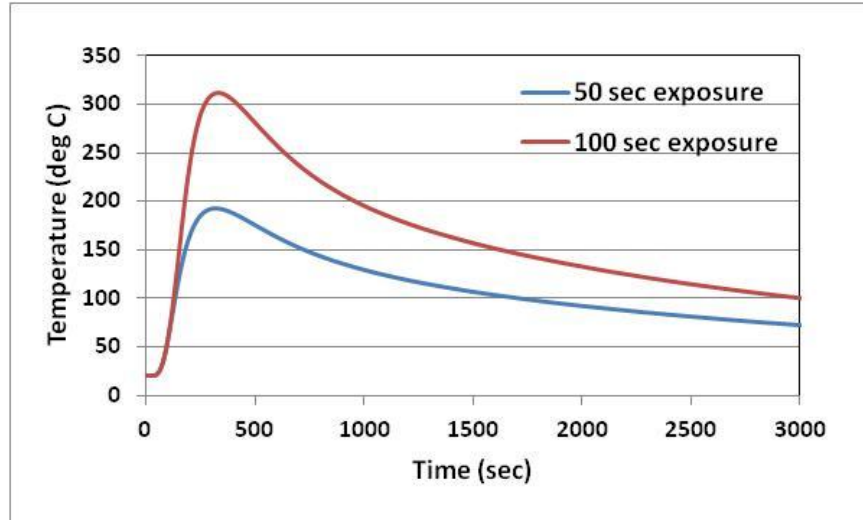**Figure 8: Peak temperature in DAS board with and without felt insulation.**

Figure 9: Temperature history for Al substructure for different arc-jet exposure time.
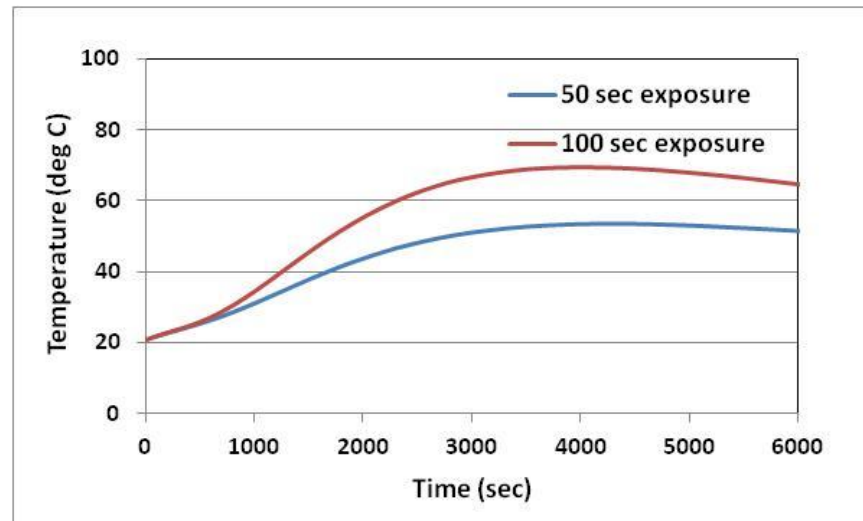

Figure 10: Temperature history for DAS board for different arc-jet exposure time.

IV. Arc-jet testing

Two arc-jet tests were conducted in the Aerodynamic Heating Facility at NASA Ames Research Center. The test articles were exposed to the arc-jet environment for 50 seconds followed by a long cool-down period. The aeroshell and payload survived the tests and there was no battery failure. Some cracks on PICA near the thermocouple plug were observed during the cool-down that were believed to be caused by thermal stresses due to CTE mismatch between the aluminum substructure and PICA. Figure 11 shows the picture of the model during and after the arc-jet test. The pre-test design elements like material selection for the substructure and payload, exposure time etc. led to a successful completion of the arc-jet test and we did not observe battery explosion or any other catastrophic failure.

We were able to obtain extensive data sets from both experiments from the facility and on-board data acquisition system. A map of those thermocouples that were used to obtain temperature histories and compare data with finite-element analysis is shown in Figure 12. One of the differences between the two tests was that in the first test the vacuum was maintained inside the probe throughout the cool-down period; whereas in the second test, once the substructure reached 60^0C, the vacuum was released and the probe was vented to ambient air. This was intentionally done in the second test to understand the effects of venting as it causes the heat to redistribute more rapidly inside the container. The details of the tests, thermocouple data, calorimeter measurements and heat flux calculations are provided in References 8 and 11. The next section describes the predictions from the higher-fidelity finite-element

American Institute of Aeronautics and Astronautics

model and compares temperature histories on the aeroshell, carrier structure, and payload with measured thermocouple data.

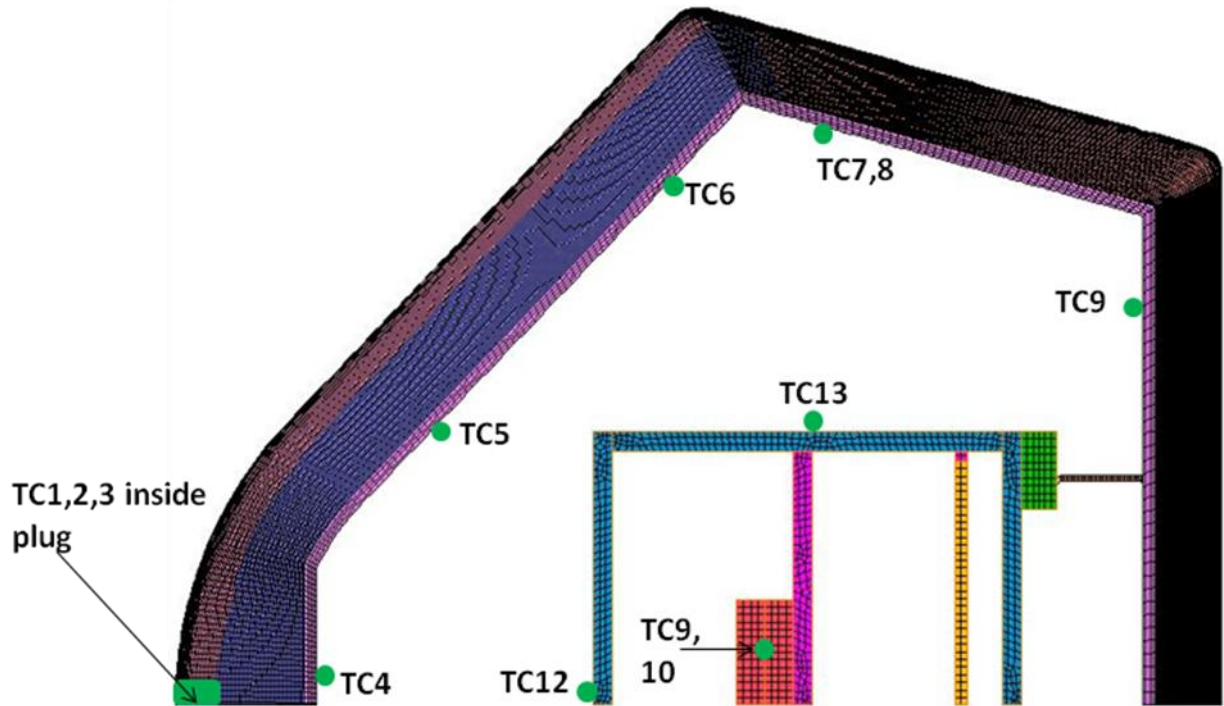**Figure 11: SPRITE model during and after the arc-jet tests.**

Figure 12: Thermocouple map.

V.   Thermal soak analysis of probe after arc-jet exposure

To predict thermal response of the TPS materials during arc-jet exposure, analysis was performed using the fully implicit thermal response code, TITAN [5]. A 2D axi-symmetric model was generated with a very fine surface mesh. To perform thermal analysis of the cool-down period after arc-jet exposure, the fidelity of finite-element analysis was improved by coupling TITAN output to the finite-element model. The grid-points corresponding to aeroshell and substructure immediately after exposure were imported to the finite-element preprocessor. The temperature contours immediately after exposure were also imported in the finite-element preprocessor and applied as initial condition to the model. The cool-down analysis was subsequently performed using the nonlinear finite-element thermal solver. This method ensured that energy dissipation due to ablation and pyrolysis of PICA during the arc-jet exposure was taken into account. The details of this approach are discussed in Section II. While some amount of pyrolysis occurred immediately after exposure, the cool down process was rapid enough that it was reasonable to

assume it will not significantly influence the thermal state of the interior and payload. The comparison of TITAN and higher-fidelity finite-element analysis predictions with measured thermocouple data near the stagnation point is shown in Figure 13. The peak temperature for TC1 that is located closest to the surface occurs immediately after the exposure at 50 seconds. TITAN shows a higher peak temperature value compared to the measured thermocouple data. There is a possibility that the temperature exceeded the operating limit of the thermocouple and caused this discrepancy. In general the TITAN predictions corresponding to in-depth thermocouple locations in stagnation plug are in good agreement with measured thermocouple data. The peak temperatures corresponding to in-depth thermocouples (TC 2 and TC3) occur a few seconds after the exposure and are predicted higher by finite-element model compared to the measured data. This discrepancy is caused by not taking into account the pyrolysis that occurs after the exposure. However, as the cool-down proceeds further, after 400 seconds, the difference becomes small and finite-element modeling seems to be in good agreement with measured data.

The temperature contours in Figure 14 show that, while immediately after the arc-jet exposure the temperature in the PICA surface is close to 2100 ^{0}C, within 50 seconds the whole forebody rapidly cools down below 700 ^{0}C. At this time the substructure and payload are still at room temperature. The substructure heating starts after 100 seconds and it peaks closer to 200 seconds. Figure 14 also shows that even after 500 seconds the payload (metal container, electronic board and batteries) stays at room temperature, and it takes several minutes before a rise in temperature occurs. There were several thermocouples mounted on the substructure, metal container box, board and the batteries to measure the internal temperature history of the probe during and after the exposure.

Temperature histories for various locations in the Aluminum substructure are shown in Figure 15. The finite-element predictions show the same trend but higher peak temperatures compared to the thermocouple data. The difference between conduction based model and this higher-fidelity finite-element model provides an estimate of the difference caused by ablation and pyrolysis during the exposure. However, the peak temperature predicted by the higher-fidelity finite-element model is still higher than the measured data. This discrepancy could be caused by not modeling pyrolysis in PICA that occurred after the exposure to the arc-jet stream.

Figure 16 shows the temperature rise in the metal container and the battery during the two tests. It takes more than 400 seconds before the temperature starts to rise in the payload. Only after an hour does it show any significant rise beyond 40°C. In the first test the vacuum was maintained during the entire cool-down period, whereas in the second test the probe was eventually vented to ambient condition after 2400 seconds. The box and battery temperatures go down slightly in the second test as the cool ambient air enters the probe.

In the finite-element analysis it was assumed that the model is not vented and vacuum was maintained throughout the cool-down period. Therefore, we could use only the first test data set for comparison with finite-element modeling predictions. The finite-element temperature predictions on the aluminum container and battery and comparison with measure thermocouple data are shown in Figure 17. The higher-fidelity post test finite-element analysis predictions are in very good agreement with the data obtained during the first test, for both the aluminum DAS container box and batteries. The thermal properties for the battery were adopted from reference 12 and 13. Reference 12 does not provide a single value for the thermal conductivity of the battery, instead, lists the thermal conductivities of various battery components. Therefore, to account for uncertainty in the thermal conductivity value for the battery, two simulations were performed with higher (5.0 W/m K) and lower conductivity (1.0W/mK) values. The simulations did not show a significant difference in temperature response. The simulations were also performed without battery heating. The simulations show that if the heat generation due to battery operation is not accounted; the rise in temperature due to arc-jet exposure is only 11°C and the battery temperature will stabilize in 2 hours at 30°C.
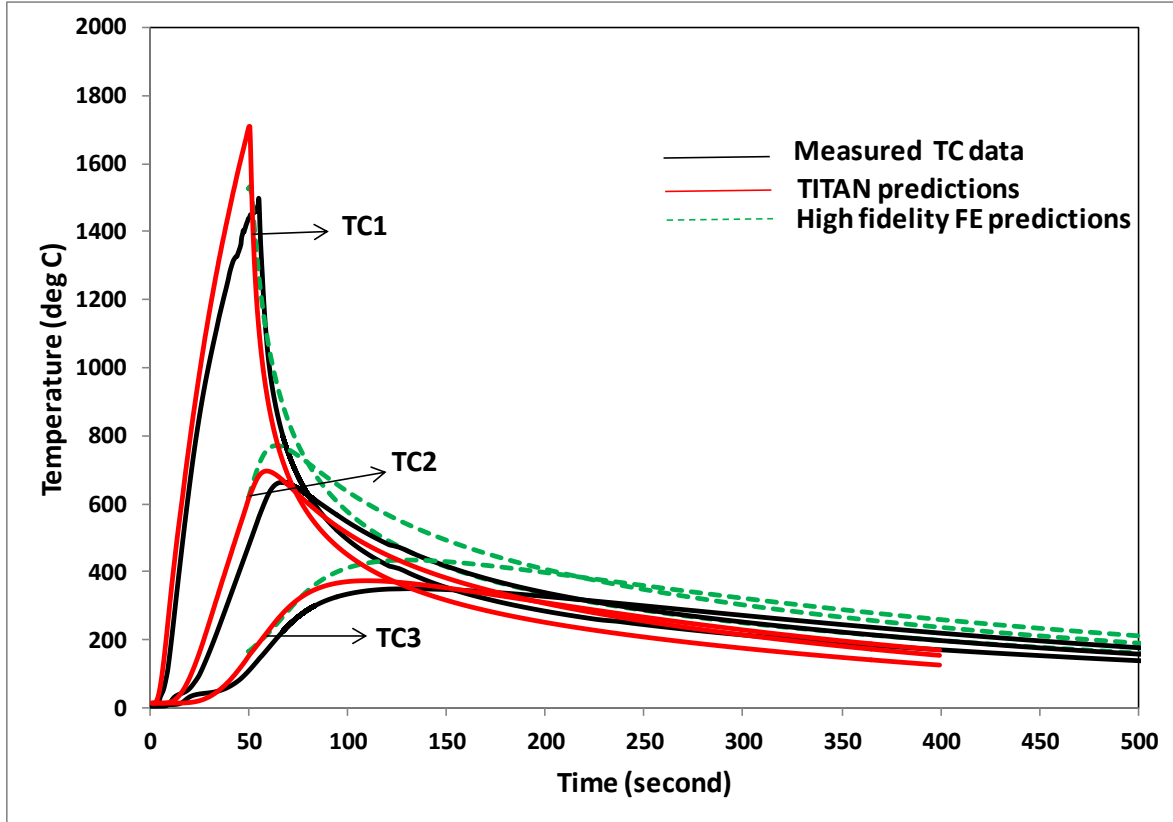
Figure 13: Comparison TITAN and finite-element predictions of temperature history near stagnation point with measured data during the cool down.
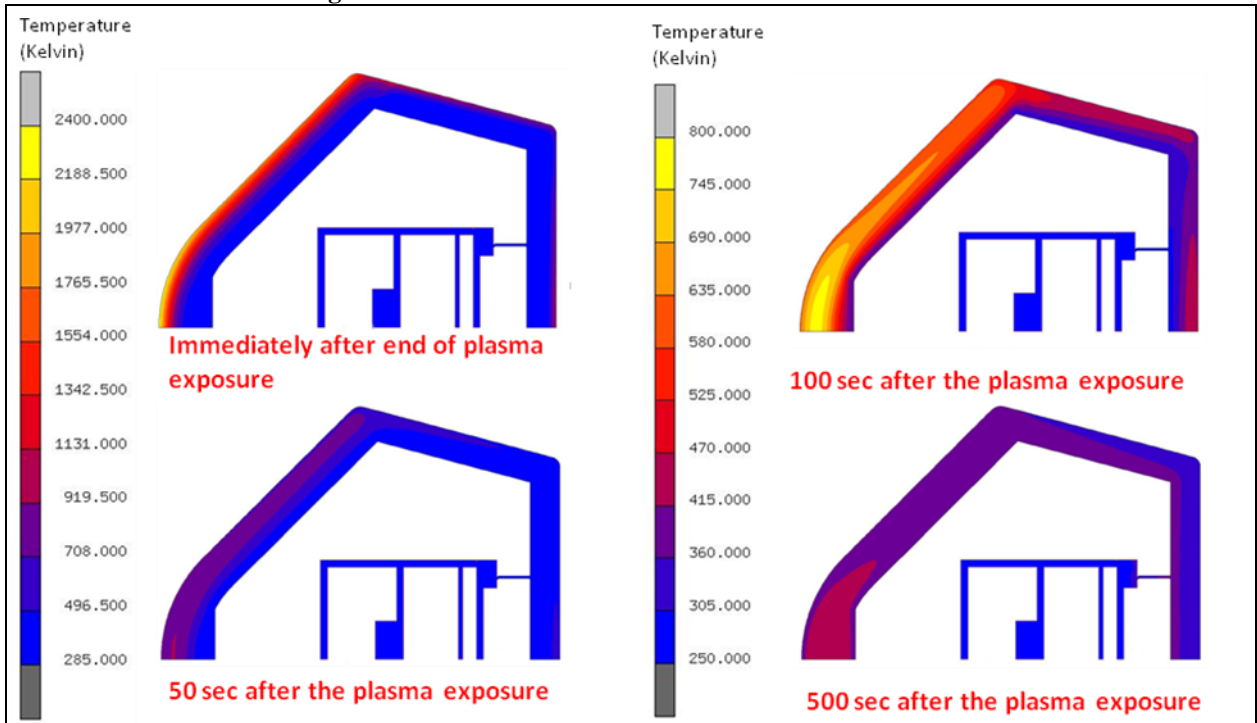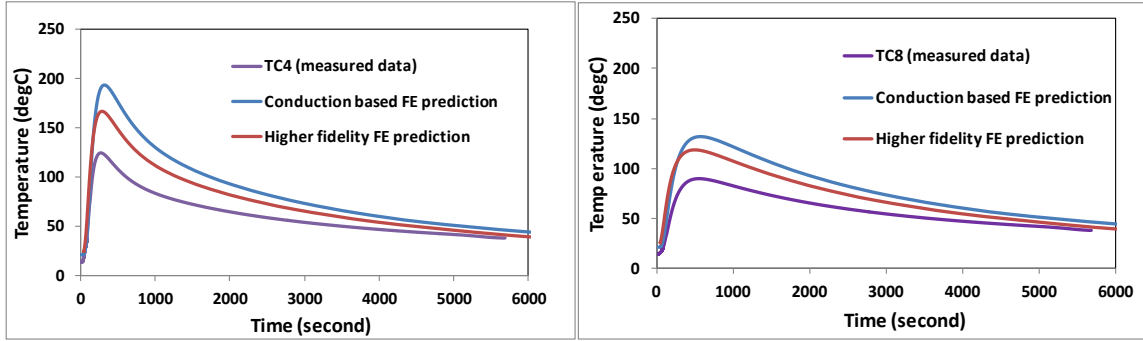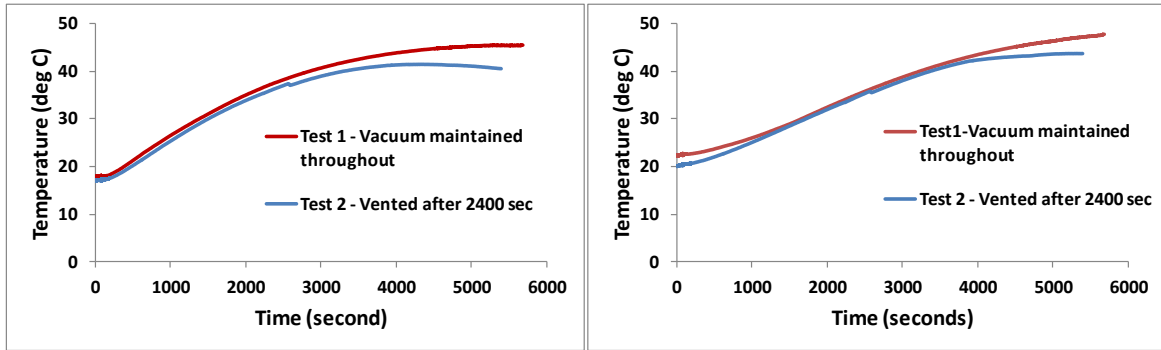

Figure 14: Temperature contours in the probe after exposure.

(a) Location: substructure below the stagnation plug (b) Location: Substructure below the back shell.
Figure 15: Temperature history for Al substructure - comparison of FE predictions with test data.

(a) TC measurements at the Al container   **(b) TC measurements at the battery.**
Figure16: Temperature history comparisons between arc-jet test1 and test2.
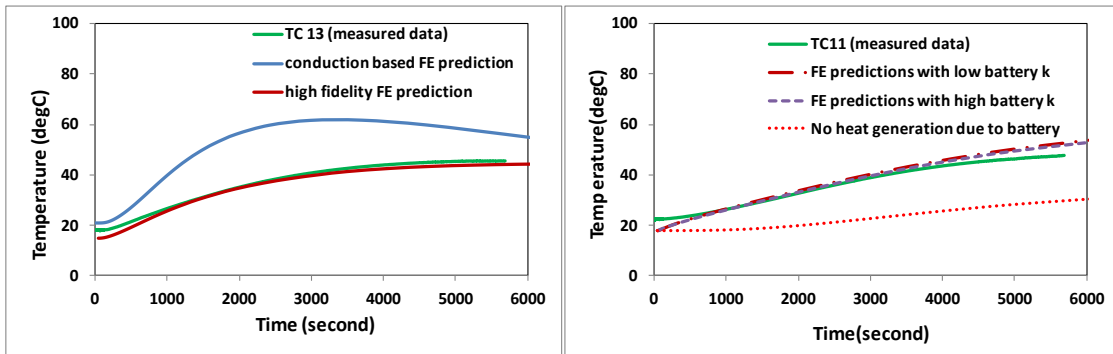
(a) Temperature predictions for the Al container   **(b) Temperature predictions for the battery**
Figure 17: Temperature history predictions at the interior of probe - comparison of FE predictions with test data.

VI. Summary and conclusions

For SPRITE, finite-element thermal analyses guided the substructure and payload materials selection, arc-jet test exposure time and thermocouple locations. The analyses were instrumental in conducting successful arc-jet tests for the SPRITE probe. The aeroshell and payload survived the arc-jet exposure; no battery explosion occurred either during or after the tests and the team was able to obtain thermocouples data from arc-jet facility and internal DAS system. Temperature history predictions for the electronics metal container box and the batteries were in good agreement with experimentally observed data. The combination of TITAN with finite-element thermal soak analysis proved to be a good methodology to provide a reasonably accurate picture of thermal energy absorption and subsequent effects on payload temperatures for small re-entry probes. Based on the confidence derived from these

results, the approach established for thermal analysis of the SPRITE probe will be extended to multi-mission Earth entry vehicle (MMEEV) thermal soak analysis.[14]

Acknowledgments

References

[1] Maddock, R. W., "Multi Mission Earth Entry Vehicle Design Trade Space and Concept Development Status", proceedings, 7th International Planetary Probe Workshop, Barcelona, Spain,14-18 June 2010.

[2] Howard, A. R., Prabhu, D.K., Venkatapathy, E., and Arnold, J. O."Small Probes as Flight Test Beds for Thermal Protection Materials" proceedings , 7th International Planetary Probe Workshop, Barcelona, Spain, 14-18 June 2010.

[3] Empey, D. M., Skokova, K.A., Agrawal P., Swanson G., Prabhu, D.K., Peterson K. H., and Venkatapathy E., "Small Probe Reentry Investigation for TPS Engineering (SPRITE)", proceedings , 8th International Planetary Probe Workshop, Portsmouth, VA, 6-10 June 2011.

[4] Wright, M., Candler, G., and Bose, D., "Data-Parallel Line Relaxation Method for the Navier–Stokes Equations," *AIAA Journal*, Vol. 36, No. 9, 1998, pp. 1603–1609.

[5] Chen, Y.-K., and Milos, F.S., "Two-Dimensional Implicit Thermal Response and Ablation Program for Charring Materials," *Journal of Spacecraft and Rockets*, Vol. 38, No. 4, July-August 2001, pp. 473-481.

[6] MSC Software Corporation, Marc Version 2008r1, 2 MacArthur Place, Santa Ana, CA 92707.

[7] Swanson et. al. "Development of an Integrated Data Acquisition System for a Small Flight Probe", proceedings**,** 50th AIAA Aerospace Sciences Meeting, Nashville, TN, January 2012.

[8] Prabhu, D. K., "Flowfield Analysis of a Small Entry Probe (SPRITE) Tested in an Arc Jet", proceedings, 50th AIAA Aerospace Sciences Meeting, Nashville, TN, January 2012.

[9] Milos, F.S., and Chen, Y.-K., "Ablation and Thermal Property Model for Phenolic Impregnated Carbon Ablator (PICA)," NASA/TM-2009-215377, Jan. 2009.

[10] Anon., "NASA-Space Shuttle Manual 1988."

[11] Skokova et.al., "Arc Jet Testing of Small Entry Probe (SPRITE)", paper submitted to 50th AIAA Aerospace Sciences Meeting, Nashville, TN, January 2012.

[12] Kim, U. S., Shin, C. B, Kim, C-S, "Modeling for the scale-up of a lithium-ion polymer battery", Journal of Power Sources vol. 189, 2009, pp. 841–846.

[13] A. Pesaran, A. A. and Keyser M., "Thermal Characteristics of Selected EV and HEV Batteries", proceedings, Annual Battery Conference: Advances and Applications, Long Beach, California, January 9-12, 2001

[14] Agrawal, P., Sepka, S. A., Venkatapathy, E., *Samareh,J. A., "*Thermal Soak Analysis of Earth Entry Vehicles" , Abstract submitted to the 43rd AIAA Thermophysics Conference, New Orleans, Louisiana June 2012.